How to cite: *Angew. Chem. Int. Ed.* **2024**, *63*, e202411010
doi.org/10.1002/anie.202411010

Polymer Chemistry

Inverse Vulcanization of Activated Norbornenyl Esters—A Versatile Platform for Functional Sulfur Polymers

*Alexander P. Grimm, Martina Plank, Andreas Stihl, Christian W. Schmitt, Dominik Voll, Felix H. Schacher, Jörg Lahann, and Patrick Théato**

Abstract: Elemental sulfur has shown to be a promising alternative feedstock for development of novel polymeric materials with high sulfur content. However, the utilization of inverse vulcanized polymers is restricted by the limitation of functional comonomers suitable for an inverse vulcanization. Control over properties and structure of inverse vulcanized polymers still poses a challenge to current research due to the dynamic nature of sulfur-sulfur bonds and high temperature of inverse vulcanization reactions. In here, we report for the first time the inverse vulcanization of norbornenyl pentafluorophenyl ester (NB-PFPE), allowing for post-modification of inverse vulcanized polymers via amidation of reactive PFP esters to yield high sulfur content polymers under mild conditions. Amidation of the precursor material with three functional primary amines (*α*-amino-*ω*-methoxy polyethylene glycol, aminopropyl trimethoxy silane, allylamine) was investigated. The resulting materials were applicable as sulfur containing poly(ethylene glycol) nanoparticles in aqueous environment. Cross-linked mercury adsorbents, sulfur surface coatings, and high-sulfur content networks with predictable thermal properties were achievable using aminopropyl trimethoxy silane and allylamine for post-polymerization modification, respectively. With the broad range of different amines available and applicable for post-polymerization modification, the versatility of poly(sulfur-*random*-NB-PFPE) as a platform precursor polymer for novel specialized sulfur containing materials was showcased.

Introduction

Desulfuration of natural gas and oil is a key step to produce the fossil fuels that drive our modern globalized civilization. Combined with the Claus process, industrial desulfuration of natural gas and oil has led to a global annual production of elemental sulfur of around 70 million tons in recent years.[1] However, the industrial demand of elemental sulfur is mainly limited to the fabrication of sulfuric acid,[2] vulcanized rubber,[3] fertilizers,[4] and niche applications, which leads to a phenomenon described as the 'excess sulfur problem'.[5] The concept of inverse vulcanization was introduced in 2013 by Chung et al., which enabled the use of elemental sulfur as feedstock for polymeric materials.[6] Inverse vulcanization is typically conducted by heating a mixture of elemental sulfur and one or more suitable unsaturated comonomers (so-called cross-linkers) to 130–185 °C in the presence or absence of a catalyst. Exposed to heat, the covalent bonds of cyclic elemental sulfur cleave homolytically, resulting in the formation of radical poly-

[*] A. P. Grimm, Dr. C. W. Schmitt, Prof. Dr. P. Théato
Institute for Biological Interfaces III (IBG-3)
Soft Matter Synthesis Laboratory
Karlsruhe Institute of Technology (KIT)
Hermann-von-Helmholtz-Platz 1, 76344 Eggenstein-Leopoldshafen (Germany)
E-mail: patrick.theato@kit.edu

M. Plank, Prof. Dr. J. Lahann
Institute of Functional Interfaces (IFG)
Soft Matter Synthesis Laboratory
Karlsruhe Institute of Technology (KIT)
Hermann-von-Helmholtz-Platz 1, 76344 Eggenstein-Leopoldshafen (Germany)

A. Stihl, Prof. Dr. F. H. Schacher
Institute of Organic Chemistry and Macromolecular Chemistry (IOMC)
Friedrich Schiller University Jena (FSU)
Lessingstraße 8, 07743 Jena (Germany)

A. Stihl, Prof. Dr. F. H. Schacher
Jena Center for Soft Matter (JCSM)
Friedrich-Schiller-University Jena (FSU)
Philosophenweg 7, 07743 Jena (Germany)

Dr. D. Voll, Prof. Dr. P. Théato
Institute for Technical Chemistry and Polymer Chemistry (ITCP)
Karlsruhe Institute of Technology (KIT)
Engesserstraße 18, 76131 Karlsruhe (Germany)

Prof. Dr. F. H. Schacher
Helmholtz Institute for Polymers in Energy Applications Jena (HIPOLE Jena)
Lessingstraße 12–14, 07743 Jena (Germany)

Prof. Dr. J. Lahann
Biointerfaces Institute
University of Michigan
2800 Plymouth Road, Ann Arbor, MI 48109 (USA)

meric sulfur chains which can be stabilized by incorporation of unsaturated cross-linkers, such as diisopropenyl benzene,[7] dicyclopentadiene,[8] or unsaturated vegetable oils.[9,10] Materials with up to 90 wt % sulfur are achievable via inverse vulcanization and have been employed in a variety of applications such as heavy metal adsorption,[8,9,11–13] infrared optics,[14,15] antibacterial surfaces,[16] thermal insulators,[17] flame retardants,[18] fertilizers,[19] healable materials,[20] and lithium-sulfur battery cathode materials.[21] Due to the relatively high temperatures necessary for inverse vulcanization polymerizations, the range of applicable unsaturated monomers (subsequently simply termed monomers) is limited to compounds with boiling points above the target reaction temperature, though some notable exceptions of inverse vulcanization in the vapor-phase have been reported.[15,22] In recent years, various concepts were introduced to increase the range of monomers suitable for inverse vulcanization, most prominently: Catalytic inverse vulcanization and photoinduced inverse vulcanization. Catalytic inverse vulcanization relies on the application of additives that lower the required temperature for efficient polymerization, while also decreasing the formation of hazardous side products.[23] Photoinduced inverse vulcanization exploits the cleavability of S–S bonds under UV irradiation, allowing the incorporation of volatile monomers in high sulfur-content materials.[24] In addition, the group of Pyun has demonstrated the use of sulfenyl chlorides as feedstock towards polysulfide containing materials using considerably lower temperatures than traditional inverse vulcanization.[25] Importantly, high control over the formation of polysulfides based on norbornene derivatives was reported by Pople et al. using an electrochemical ring-opening polymerization approach at ambient temperature. This method proved applicable for water soluble polysulfides with the ability for post-polymerization modification (PPM).[26] Due to the dynamic nature of polysulfides, modification of high sulfur content materials via dynamic covalent polymerization (DCP) has also proven to be a useful method to tune material properties towards desired applications.[27,28] However, as a consequence of the typically harsh reaction conditions of inverse vulcanization reactions, the amount of functional groups able to survive the polymerization conditions is limited. One method to create functional inverse vulcanized polymers, or tune their properties towards a desired application, is the post-polymerization modification of reactive precursors. Early examples of PPM on inversed vulcanized polymers include nucleophilic substitution of pendant chain leaving groups,[29] photochemical cross-linking,[30] dynamic covalent polymerization,[28] *Friedel–Crafts* cross-linking,[31] and silane polycondensation.[32,33] However, despite the progress made in opening the field of inverse vulcanization and controlling material properties, the development of a fundamental synthetic platform from which further material specialization can be achieved remains challenging.

In this work, we present the inverse vulcanization of activated norbornenyl esters, a straightforward strategy to synthesize high sulfur content materials that can be utilized as a platform for further specialization. We hypothesized that by combining the amidation of norbornenyl pentafluorophenyl ester with inverse vulcanization, a versatile, high sulfur content polymer would be achievable which can then easily be modified toward desired materials applications.[34] The utility of the presented method is demonstrated by modifying the inverse vulcanized precursor polymer poly(sulfur-*random*-norbornenyl pentafluorophenyl ester), abbreviated poly(S-*r*-NB-PFPE), with three different functional primary amines: *α*-amino-*ω*-methoxy poly(ethylene glycol) (Amino-mPEG), aminopropyl trimethoxy silane (APTMS), and allylamine (AA) (refer to Scheme 1). On the one hand, modification with Amino-mPEG and APTMS allows the transformation of the precursor polymer into materials applicable for i.e., surface coatings and particle formation. On the other hand, the amidation of poly(S-*r*-NB-PFPE) allows for the introduction of reactive groups that would normally not survive the harsh conditions of an inverse vulcanization, demonstrated by the use of allylamine. The synthetic routes described herein emphasize the versatility and potential of the material platform presented in this work.

Results and Discussion

Inverse Vulcanization

Norbornenyl pentafluorophenyl ester was synthesized according to literature and the successful preparation was confirmed by nuclear magnetic resonance (NMR) and infrared (IR) spectroscopy (refer to SI, Figures S1–S3).[35] The norbornenyl compound was chosen as active ester over the analogous acrylate derivative for two reasons: First, acrylates have been found to be unreactive in inverse vulcanization without catalysts compared to non-polar

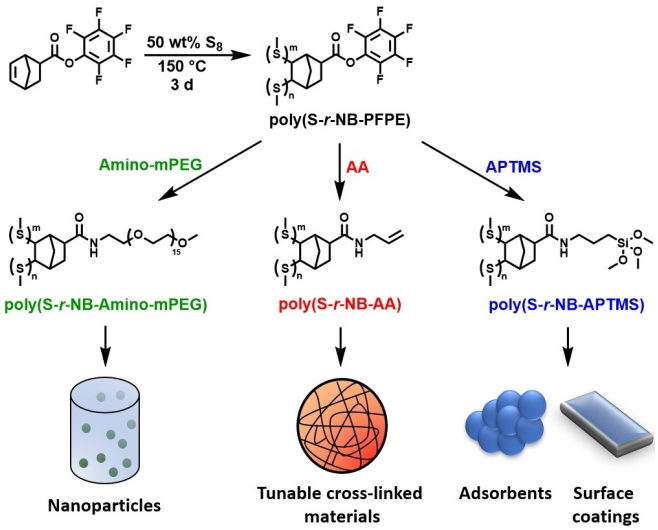

Scheme 1. Reaction scheme of the inverse vulcanization of norbornenyl pentafluorophenyl ester (PFPE) with elemental sulfur. Subsequent amidation of the reactive PFP ester allows the sulfur precursor polymer to be used in a wide range of applications.

molecules.[23] Secondly, norbornenes have been reported before to undergo inverse vulcanization effectively.[32] Poly(sulfur-*random*-norbornenyl pentafluorophenyl ester) (poly(S-*r*-NB-PFPE)) was synthesized by reacting equal masses of elemental sulfur and norbornenyl pentafluorophenyl ester at 150–170 °C for different times to evaluate the best reaction parameters (refer to Figure 1A). Full conversion of norbornenyl C=C double bonds was confirmed via ^{1}H- and ^{13}C NMR spectroscopy after a reaction time of 4 h at 150 °C. The respective ^{1}H NMR spectrum of poly(S-*r*-NB-PFPE) showed no resonances in the range between 6.5 and 6 ppm referring to the norbornenyl C=C double bond while resonances of aromatic C=C double bonds were confirmed via ^{13}C NMR spectroscopy in the range of 137 to 143 ppm (refer to SI, Figure S4 and S5). However, differential scanning calorimetry (DSC) measurements showed full conversion of elemental sulfur only after 3 days of reaction time as indicated by the absence of a melting peak in the region of 110–120 °C, which is attributed to the melting of residual elemental sulfur (T_m = 112 °C) (refer to Figure 1B). Additionally, the T_g of poly(S-*r*-NB-PFPE) was found to increase with longer reaction times from -2 °C after reacting for 4 hours to 32 °C after a reaction time of 3 days. The increase in glass transition temperature (T_g) with the reaction time indicated the progression of sulfur conversion, as the material became more stable due to higher molecular weight with increasing amounts of incorporated sulfur. Furthermore, increasing the reaction temperature to 160 and 170 °C, respectively, did not prove to accelerate the conversion of elemental sulfur. Regardless of the temperature, 3 days of reaction time were necessary to reach full sulfur conversion (refer to SI, Figure S6). The influence of reaction temperature and time was further evaluated in regard to molecular weight and the stability of the active PFP ester in the polymer. The behavior of the molecular weight of poly(S-*r*-NB-PFPE) with increasing reaction time and temperature was investigated utilizing size exclusion chromatography (SEC). The SEC traces showed the formation of oligomers after 4 hours. Interestingly, the molecular weight distribution was found to be similar for all polymers, regardless of the reaction temperature indicating a controlled formation of an oligomeric species (refer to Figure 1C). After 24 hours, the molecular weight distributions of the reaction mixtures synthesized at 150, 160, and 170 °C showed a slight broadening. Finally, after 3 days the influence of the reaction temperature became more pronounced, especially for the reaction mixture at 170 °C, showing a broad molecular weight distribution with significant higher molecular weight compared to reaction at lower temperature. This can be explained by the occurrence of additional cross-linking taking place via substitution of aromatic PFP rings (refer to SI, Figure S7 and Table S1).[36] It was found that upon elevating the reaction temperature from 150 to 160 °C and 170 °C, the formation of pentafluorophenol as the by-product increased, which was detected by ^{19}F NMR spectroscopy (refer to Figure 1D). We hypothesized that aromatic side reactions were due to the nucleophilic character of radical S$^{\bullet}$ species that were formed during inverse vulcanization at high temperatures. Thus, the reaction temperature for the preparation of poly(S-*r*-NB-PFPE) should ideally not exceed 150 °C to prevent damaging the PFP moieties via nucleophilic substitution or radical abstraction of aromatic fluorine atoms and to avoid thermal decomposition of NB-PFPE.[37] Noteworthy, the formation of norbornene derived polysulfides was recently studied in a work by Pople et al. who demonstrated the tendency of norbornenes to form cyclic trisulfides that undergo electrochemical[26] as well as anionic polymerization.[38] These norbornene derived polysulfides were shown to be depolymerizable under high temperature, opening a potential pathway towards recyclability of high sulfur content materials based on norbornene building blocks.[26] We therefore hypothesize that the reaction is taking place via a cyclic intermediate which further reacts under ring-opening to form poly(S-*r*-NB-PFPE). It can be concluded that norbornenyl pentafluorophenyl ester can withstand reaction conditions of an inverse vulcanization in a controlled manner at elevated temperatures while maintaining its unique reactive functionality. However, temperatures higher than 150 °C need to be avoided to prevent additional crosslinking due to the reactive aromatic fluorinated esters and depolymerization. This developed synthesis strategy thus opens the pathway to a sustainable and versatile material platform through simple PPM via the active ester of the novel, highly sulfur-containing precursor polymer. Polymers bearing activated PFP ester moieties are known to quantitatively undergo amidation reactions with primary or secondary amines under mild conditions, which allows to introduce new

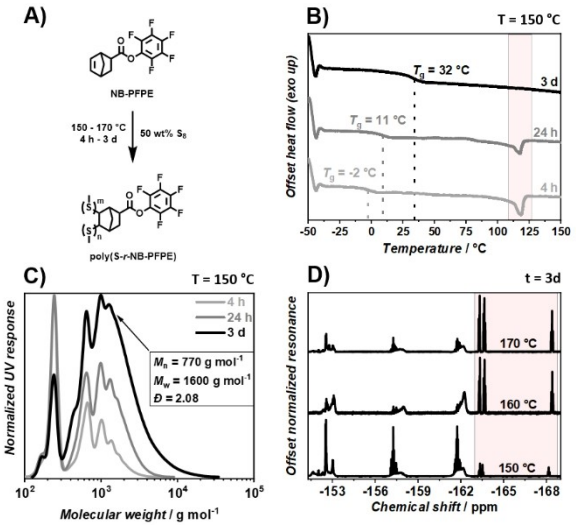

Figure 1. A) General reaction Scheme of the inverse vulcanization of NB-PFPE giving poly(S-*r*-NB-PFPE). B) DSC thermograms of poly(S-*r*-NB-PFPE) after 4 h, 24 h, and 3 d of reaction time, respectively. After 3 d, no more melting of residual crystalline sulfur was detected in the highlighted temperature range. C) SEC traces of poly(S-*r*-NB-PFPE) after 4 h (light gray), 24 h (gray), and 3 d of reaction time. Low molecular weight species decreased in intensity over time; calibration: polystyrene. D) ^{19}F NMR spectra of poly(S-*r*-NB-PFPE) after 3 d of reaction time at 150 °C (bottom), 160 °C (middle), and 170 °C (top). The presence of pentafluorophenol was found by characteristic resonances in the highlighted area.

functionalities to the sulfur polymers or tune their properties.[39] However, it is known that in the presence of amines, polysulfides are prone to nucleophilic activation that promotes dynamic S–S bond cleavage.[40] In order to confirm that norbornene-derived polysulfides are not destroyed in the presence of primary amines, a control experiment was conducted by exposing literature-known poly(sulfur-*random*-dicyclopentadiene) (poly(S-*r*-DCPD)) to benzyl amine.[8,41,42] No decrease in molecular weight or a significant change in T_g was observed, indicating that no amine-induced cleavage of polysulfides took place under the chosen conditions (detailed experimental procedure can be found in the SI, refer to Figure S10). Given the stability of norbornene-derived polysulfides, we have selected three commercially available primary amines featuring different functional groups to demonstrate the versatility of poly(S-*r*-NB-PFPE) as a platform material for various applications via selective amidation of the active ester.

Amino-mPEG

Due to the hydrophobic nature of polysulfides on the one hand, and the hydrophilic character of polyethylene glycol (PEG) on the other hand, we hypothesized that PEGylation of the poly(S-*r*-NB-PFPE) precursor can be utilized to trigger phase separation of the resulting material in aqueous media (refer to Figure 2A). However, the high polarity of PEG complicates the direct inverse vulcanization of PEGylated monomers with elemental sulfur and requires the use of a catalyst in terpolymer systems.[43,44] To circumvent this issue and create a PEG-containing polysulfide material, PPM of poly(S-*r*-NB-PFPE) with Amino-mPEG was conducted. Substitution of the active PFP esters of poly(S-*r*-NB-PFPE) with 1.2 eq Amino-mPEG was carried out in

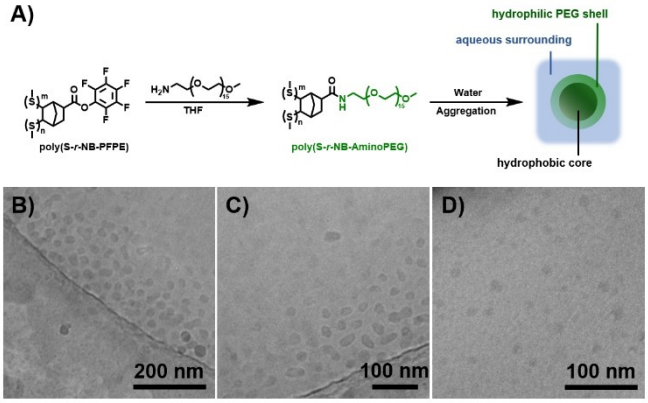

Figure 2. A) Schematic preparation of poly(S-*r*-NB-Amino-mPEG) by amidation of poly(S-*r*-NB-PFPE) followed by particle formation. In an aqueous environment, poly(S-*r*-NB-Amino-mPEG) is able to form spherical particles with hydrophobic cores and hydrophilic shells. B–D) Cryo-TEM images of poly(S-*r*-NB-Amino-mPEG) particles with different magnifications. In aqueous environments, nanometer scale particles were observed (mean radius: 12 ± 2 nm). The sharp line seen in B) and C) is the edge of a grid hole of the sample holder. The particles mainly accumulate on the edge of the ice film.

solution, followed by precipitation (refer to SI). ^{19}F NMR spectroscopy of the resulting material showed no residual resonances in the range from −152.5 to −162.5 ppm, indicating the complete conversion of aromatic PFP ester groups (refer to SI, Figure S11) while the respective ^{1}H- and ^{13}C NMR spectra showed strong resonances in the region of 3–4 ppm and 71–73 ppm, respectively, which was attributed to the presence of PEG backbone protons (refer to SI, Figure S12 and S13).[45] No sulfuration of ester groups toward thioesters or thiones was found in the ^{13}C NMR spectrum of poly(S-*r*-NB-Amino-mPEG), indicating the selective amidation of active esters to be the favored reaction. Additionally, FT-IR spectroscopy revealed the full disappearance of the characteristic ester C=O vibration band at 1778 cm^{-1}, while the formation of the proposed amide bond was confirmed by the presence of the amide C=O vibration band at 1665 cm^{-1}. The IR spectrum of poly(S-*r*-NB-Amino-mPEG) also showed strong characteristic C–H and C–O vibration bands at 2864 and 1095 cm^{-1}, respectively (refer to SI, Figure S14).[46] SEC elugrams of poly(S-*r*-NB-Amino-mPEG) showed an increase of molecular weight from $M_n \approx 770$ g mol^{-1} to 3200 g mol^{-1} after the amidation. Although the molecular weights are subject to error as they were measured relative to polystyrene standards,[6] the comparison between the elugrams of poly(S-*r*-NB-PFPE) and poly(S-*r*-NB-Amino-mPEG) showed a 4.2-fold increase in M_n, which was consistent with the calculated increase (4.1-fold) for complete PFP ester conversion with the chosen $M_n = 750$ g mol^{-1} Amino-mPEG. Additionally, precipitation proved to effectively remove low molecular species from the product, which resulted in a decrease of $Đ$ from 2.11 to 1.60 (refer to SI, Figure S15). Thermal properties of poly(S-*r*-NB-Amino-mPEG) had been characterized via thermogravimetric analysis (TGA) as well as DSC. The thermal decomposition profile of poly(S-*r*-NB-Amino-mPEG) revealed an increase of $T_{5\%}$ from 168 °C to 234 °C compared to the precursor polymer poly(S-*r*-NB-PFPE), which was derived from the substantial amount of PEG in the material and confirms the quantitative conversion of PFP esters (refer to SI, Figure S16).[47] DSC measurements of poly(S-*r*-NB-Amino-mPEG) revealed an expected melting area of 32–58 °C in the first heat run, which shifted to lower temperatures (25–51 °C) in the second heat run and was attributed to the melting of crystalline PEG segments (refer to SI, Figure S17).[48] The shift of the melting area in the second heat run toward lower temperatures is believed to be caused by the fast formation of small crystallites during the cooling step, which have a smaller melting temperature, compared to fully grown equilibrated crystallites.[49] Due to the hydrophobic nature of polysulfides and norbornenes on the one hand, and the hydrophilic character of PEG chains on the other hand, we hypothesized that agglomeration could be triggered, when bringing poly(S-*r*-NB-Amino-mPEG) in aqueous media (refer to Figure 2A). We proposed a micelle structure with sulfur/norbornene agglomerates in the core and PEG chains closer to the surface, acting like a sort of corona. Samples were prepared by dissolving poly(S-*r*-NB-Amino-mPEG) in a mixture of THF/H_2O (1:1 v/v) to obtain a polymer

concentration of 3.5 mg mL^{-1}. Aggregate formation was triggered by slowly evaporating the THF in an open vial overnight, thereby increasing the aqueous fraction and forcing the sulfur segments to phase separate. Dynamic light scattering (DLS) measurements of the resulting suspension revealed the presence of aggregates with a hydrodynamic radius of 17 nm and a narrow dispersity (refer to SI, Figure S18). Due to the fact that the proposed micelle structure is only persistent in aqueous media, cryogenic transmission electron microscopy (cryo-TEM) was performed in order to investigate the structure of the aggregates. Figure 2B–D show the cryo-TEM images of poly(S-*r*-NB-Amino-mPEG) aggregates. The formed particles were spherical in shape, with a mean radius of 12 nm (standard deviation (SD): 2 nm), which was in accordance with the size determined by DLS. Interestingly, no ordered structures were observed under regular, dry TEM conditions (refer to SI, Figure S19), indicating destruction of particles under non-aqueous conditions, which may open a pathway toward controlled capture and release of substances via changing polarity or dryness of the surrounding environment of poly(S-*r*-NB-Amino-mPEG). Nevertheless, the presented strategy proved to be applicable for inducing phase separation of sulfur polymers in aqueous media by PPM with hydrophilic PEG chains. The straightforward preparation of spherical, hydrophilic nanoparticles derived from otherwise hydrophobic high sulfur content polymers via amidation of active PFP esters with Amino-mPEG moieties, substantiates the applicability of poly(S-*r*-NB-PFPE) as a platform material for controlled transport of sulfur micelles in aqueous environments for future applications such as homogeneous heavy metal capture or drug delivery.[44,50]

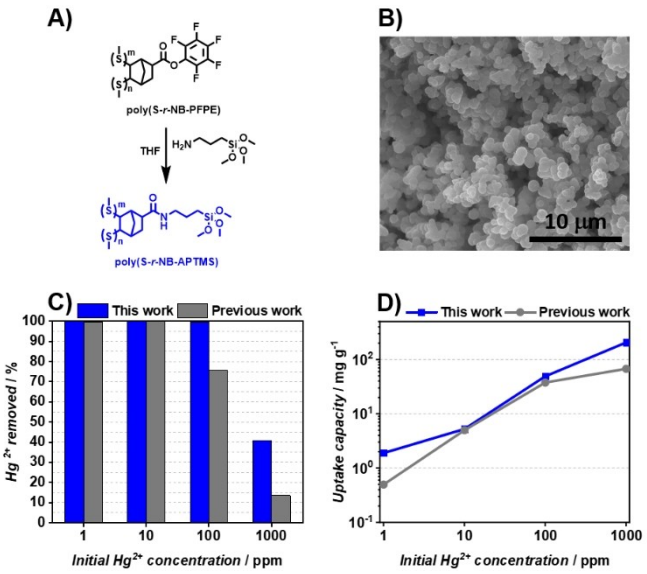

Figure 3. A) Synthesis scheme of poly(S-*r*-NB-APTMS) (blue) by amidation of poly(S-*r*-NB-PFPE) with APTMS in THF under ambient conditions. B) SEM image of spherical poly(S-*r*-NB-APTMS) particles. Average diameter: 810 nm (SD: 215 nm). C) and D) Removed Hg^{2+} ions and uptake capacity for Hg^{2+} ions of poly(S-*r*-NB-APTMS) particles from aqueous solution depending on the initial concentration of Hg^{2+} ions in comparison to our previous study.[11] For each adsorption test, 100 mg poly(S-*r*-NB-APTMS) particles in 50 mL $HgCl_2$ (c = 1–1000 ppm) solution were used, respectively.

Aminopropyl Trimethoxy Silane

Trialkoxysilanes are an important class of chemicals used for functionalization of glass, metals, silica, or even sand and organosilanes play a vital role as coupling agents for surface coatings,[51] magnetic materials,[52] cross-linkers,[53] as well as adsorption materials.[54] To make the field of silane chemistry available to our precursor polymer, amidation of poly(S-*r*-NB-PFPE) with aminopropyl trimethoxy silane (APTMS) was carried out using 1.20 eq of APTMS, yielding poly(S-*r*-NB-APTMS) (Refer to Figure 3A). However, due to the rapid polycondensation of methoxy silanes, the obtained polymer was kept in dry solution until further use. Based on our previous study, the applicability of poly(S-*r*-NB-APTMS) for the synthesis of sulfur-containing silica particles as mercury adsorbent was investigated.[13] For this, poly(S-*r*-NB-APTMS) in THF was added to a mixture of aqueous ammonia in ethanol at ambient temperature (refer to SI). A precipitate was observed in the reaction mixture after a few seconds, indicating the formation of insoluble silica particles FT-IR analysis of purified poly(S-*r*-NB-APTMS) particles proved the successful amidation of PFP ester groups by disappearance of the ester C=O vibration band at 1779 cm^{-1} and the appearance of the amide C=O vibration band at 1640 cm^{-1} (refer to SI, Figure S20). Additionally, an increase in C–H vibration band intensity was observed in the range of 3000–2800 cm^{-1}, which indicated the incorporation of propyl CH_2-groups into the material. From the very strong and broad absorbance band of the asymmetric Si–O–Si stretching vibration at 1090 cm^{-1}, the formation of a cross-linked siloxane network was concluded, which was in line with the expectations.[55] Additional TGA, DSC, Brunauer–Emmett–Teller (BET) data is provided in the Supporting Information (Figure S21–S23) to support the findings. Scanning electron microscopy (SEM) of poly(S-*r*-NB-APTMS) particles revealed spherical particles with an average diameter of 810 nm (SD: 215 nm) (refer to Figure 3B and the SI, Figure S24). The high standard deviation was caused by the broad molecular weight distribution of the precursor material, resulting in particles of higher size distribution. However, elemental analysis (EA) revealed a final sulfur content of poly(S-*r*-NB-APTMS) particles of 37 wt %, which was twice the amount compared to the particles of the inverse vulcanization of trimethoxyvinylsilane reported in an earlier work.[13] One of the major applications of polymers derived from inverse vulcanization is their use as heavy metal adsorbents. Most notably, the affinity of polysulfides towards environmentally hazardous mercury ions is an extensive field of research in materials science.[56] Applicability of poly(S-*r*-NB-APTMS) particles as mercury adsorbent was evaluated in aqueous solutions of Hg^{2+} at different concentrations. Four solutions of $HgCl_2$ in 50 mL deionized (DI) water were prepared with initial Hg^{2+} concentrations of 1, 10, 100, and 1000 ppm,

respectively. 100 mg poly(S-*r*-NB-APTMS) particles were added to each solution under vigorous stirring. After 24 h at ambient temperature, the particles were filtered off and the remaining Hg^{2+} concentrations were determined via cold vapor atomic absorption spectroscopy (CV-AAS). It was found that for initial concentrations of 1–100 ppm Hg^{2+}, over 99 % of mercury could be removed from aqueous solutions. At an initial Hg^{2+} concentration of 1000 ppm, 40.8 % of mercury could still be removed, which represents a remarkable improvement compared to our earlier study (refer to Figure 3C and 3D). The improved adsorption of Hg^{2+} was attributed to the increased amount of sulfur incorporated in the particles as well as the presence of coordinating amide groups.[13,57] Furthermore, distribution coefficients and uptake capacities of poly(S-*r*-NB-APTMS) particles were determined and can be found in the Supporting Information (Figure S25 and Table S2).

As reported previously, inverse vulcanized polymers carrying hydrolyzable silane groups can be utilized to produce sulfur coatings by dip or spin coating,[12] in which poly(S-*r*-NB-APTMS) was applied as coating material on silicon surfaces to validate the silane coupling chemistry. Consequently, the amidation solution of poly(S-*r*-NB-PFPE) with APTMS was directly employed for spin coating on silicon wafers (parameters can be found in the SI). Surfaces with one, two, and three coating cycles were prepared, and surfaces were cleaned with ethanol after each cycle. The thicknesses of poly(S-*r*-NB-APTMS) coatings were determined by ellipsometry. Notably, the film thicknesses increased with increasing number of spin-coating cycles from 317, over 410, to 422 nm after one, two, and three coating cycles, respectively (refer to Table 1). However, the resulting coating thicknesses did not increase linearly with the number of coating cycles which is likely caused by the dissolution of deposited material upon subsequent layer addition.

Thicknesses of poly(S-*r*-NB-APTMS) coatings were found to be in the same region as previously reported spin coatings of inverse vulcanized polymers and can be explained by the relatively high polymer concentration of the spinning solution ($0.1\,g\,mL^{-1}$). Hydrophobicity of poly(S-*r*-NB-APTMS) coated silicon wafers was evaluated by water contact angle measurements. The static water contact angle was found to increase from $47.7\pm1.8°$ of the clean silicon wafer to around 86° when coated with poly(S-*r*-NB-APTMS), independent of the number of coating steps (refer to Table 1). To confirm the presence of the amide binding motif and polysulfides of poly(S-*r*-NB-APTMS) and elucidate the homogeneity of the coating, time-of-flight secondary ion mass spectrometry (ToF-SIMS) was performed on spin-coated silicon wafers. In accordance with our earlier study, S_2^- and S_3^- fragments were found to be the predominant sulfur species, while no fragments larger than S_4^- were detected in significant amounts (refer to Figure 4A).[12] It is noteworthy that due to the lower binding energy of larger $S_{n>4}^-$ fragments, they were likely to have been further fragmented and therefore were detected as smaller S^-, S_2^-, and S_3^- fragments during ion cluster bombardment.[58] Thus, the presence of polysulfide species $S_{n>4}$ cannot be ruled out. However, surface S_n^- fragment mapping revealed the distribution of sulfur to be homogeneous for all traced fragments (refer to Figure 4B and the SI, Figure S26 and S27). Additionally, ToF-SIMS has been employed for depth profiling of poly(S-*r*-NB-APTMS) coated silicon wafers, which showed homogeneous distribution of the associated polymer fragments. Presence of CNO^- fragments proved the formation of amide bonds while $SiCHO^-$ fragments can be attributed to the presence of methoxy silane groups on top of the silicon wafer (refer to Figure 4C and the SI, Figure S28). Interestingly, sulfur coated silicon wafers exhibited visible coloration from green, over blue, to purple which can be explained by thin-film interference between reflected light waves.[59] Digital microscopy revealed some inhomogeneity in the surface coatings.

Table 1: Film thicknesses and water contact angles of poly(S-*r*-NB-APTMS) coated on silicon wafers via spin-coating. Increasing the number of coating cycles increased the resulting thickness of the coating but has no impact on the water contact angle. Spinning speed = 1500 rpm, t = 15 s, uncertainty given from standard deviation of 4 and 10 measurements of ellipsometry and water contact angle, respectively.

Coating cycles	Coating thickness/nm	Static water contact angle/°
0	–	47.7 ± 1.8
1	317 ± 9	86.0 ± 0.9
2	410 ± 9	85.6 ± 0.9
3	422 ± 4	86.8 ± 1.0

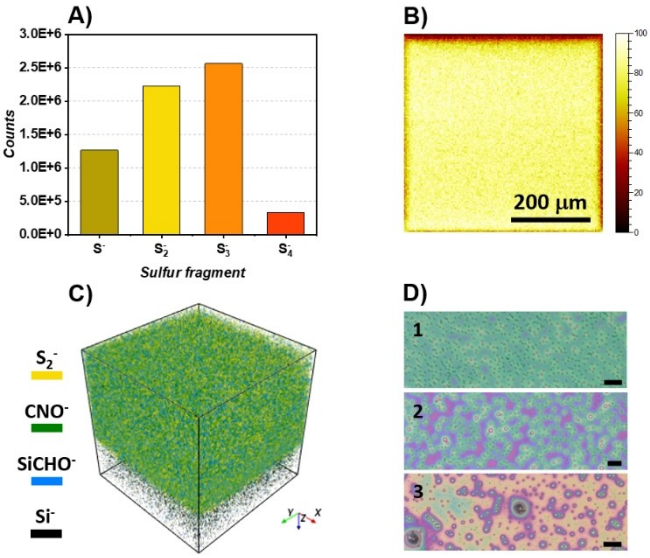

Figure 4. A) ToF-SIMS analysis of silicon wafers spin-coated with poly(S-*r*-NB-APTMS), confirming the presence of polysulfide species with S_2^- and S_3^- being the predominant sulfur rank. B) S_3^- fragment mapping via ToF-SIMS showing homogeneous distribution of sulfur on the surface. Scalebar is 200 µm. C) 3D representation of S_2^-, CNO^-, $SiCHO^-$, and Si^- fragment distribution determined via ToF-SIMS. The spin-coated poly(S-*r*-NB-APTMS) is clearly distinguishable from the silicon wafer. D) Digital microscopy images of silicon wafers coated with poly(S-*r*-NB-APTMS) with 1, 2, and 3 coating cycles, respectively. The coloration is caused by thin film interference. Scalebars are 10 µm.

Spherical pores in the micrometer range were found on all surfaces which are believed to have formed by polymerization induced self-assembly of siloxanes and THF evaporation (refer to Figure 4D).[12] Given the outstanding performance of poly(S-*r*-NB-APTMS) particles for remediation of toxic Hg^{2+} ions from water and the good homogeneity of poly(S-*r*-NB-APTMS) when coated on surfaces, we believe the amidation of poly(S-*r*-NB-PFPE) with amino silanes to be a promising strategy towards novel high sulfur content materials derived from inverse vulcanization of activated esters.

Allylamine

Due to the harsh radical conditions of typical inverse vulcanizations (i.e., radical sulfur melt at ca. 150 °C), unsaturated compounds cannot be employed in the inverse vulcanization step, when double or triple bonds ought to remain after the inverse vulcanization. Therefore, PPM has to be utilized to incorporate unsaturated moieties into inverse vulcanized polymers. Analogous to the synthesis of poly(S-*r*-Amino-mPEG) and poly(S-*r*-NB-APTMS) described above, poly(S-*r*-NB-PFPE) was reacted with 1.20 eq of allylamine (AA) at ambient temperature (refer to Figure 5A). ^{1}H- and ^{13}C NMR spectroscopy of poly(S-*r*-NB-AA) showed the appearance of resonances in the region of 5–6 ppm and at 115 and 136 ppm, respectively with can be attributed to allylic double bonds while the ^{19}F NMR spectrum revealed the disappearance of aromatic PFP resonances (refer to the SI, Figure S29–S31). Additionally, IR spectroscopy confirmed the successful reaction by appearance of a broad amide N–H stretch vibration band at 3286 cm^{-1} as well as a band at 3076 cm^{-1} which was attributed to the allyl C–H stretch vibration (refer to the SI, Figure S32). The intensity of the saturated C–H stretch vibration band at around 2955 cm^{-1} was found to increase while the characteristic C=O amide and C=C bond stretch vibrations at 1638 cm^{-1} replaced the ester bond vibration at 1776 cm^{-1}. Furthermore, a C=C bend vibration could be detected at 915 cm^{-1}, further confirming the successful amidation of the PFP esters with AA. The molecular weight of poly(S-*r*-NB-AA) was determined via SEC and found to be $M_w = 1200\ g\,mol^{-1}$ ($Đ = 1.62$), which resembles an estimated weight loss of 25 % from the poly(S-*r*-NB-PFPE) precursor polymer ($M_w = 1600\ g\,mol^{-1}$, $Đ = 2.08$) (refer to SI, Figure S33). The theoretical expected weight loss of poly(S-*r*-NB-PFPE) when assuming full amidation of PFP esters with AA was calculated to 22 %, which allows us to conclude the successful synthesis of poly(S-*r*-NB-AA) from our platform material poly(S-*r*-NB-PFPE). To evaluate the applicability of poly(S-*r*-NB-AA) for further modification on the double bond, thiol-ene reaction of the allyl species with benzyl mercaptan was conducted using AIBN at 60 °C.[60] Unfortunately, the thiol-ene reaction of poly(S-*r*-NB-AA) with benzyl mercaptan yielded unsatisfactory results. Only analytical amounts were obtained after precipitation and SEC analysis revealed the M_w to be around 600 $g\,mol^{-1}$, which is contrary to the proposed addition of benzyl mercaptan (refer to SI, Figure S34) but rather is an indication of a partial degradation. Even though ^{1}H NMR spectroscopy proved the incorporation of aromatic species in the polymer, we assume the radical mechanism of the thiol-ene reaction to destroy the polysulfur chains, leading to the decrease in molecular weight (refer to SI, Figure S35). The detailed procedure and analytics of the thiol-ene

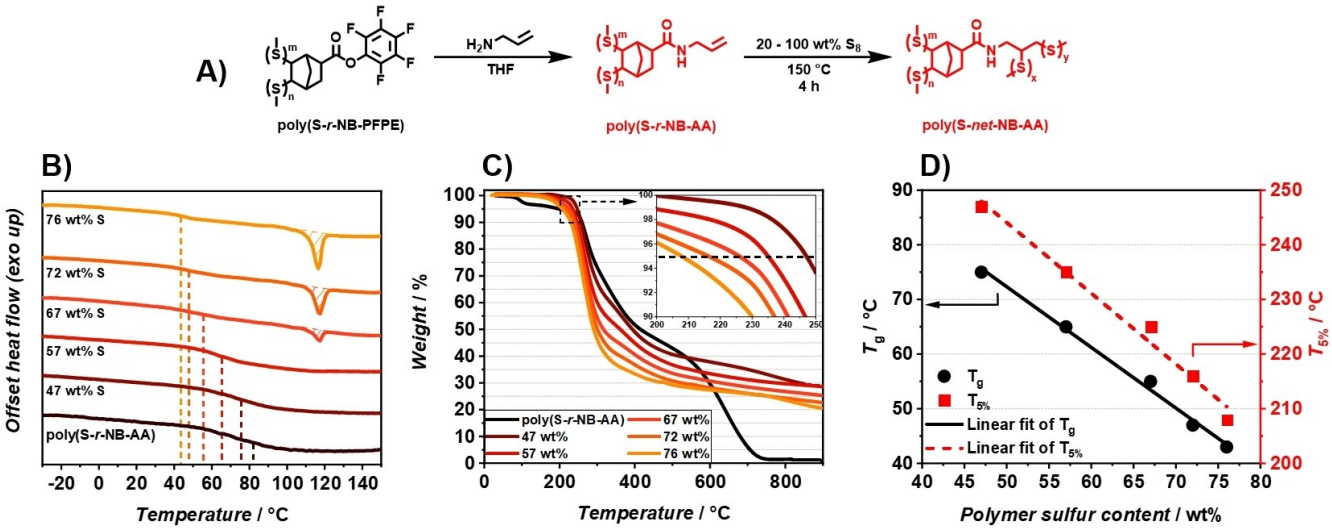

Figure 5. Synthesis and thermal analysis of cross-linked poly(S-*net*-NB-AA). A) The second cross-linking step was carried out by dry-mixing different amounts of elemental sulfur with poly(S-*r*-NB-AA) and heating to 150 °C for 4 h. DSC thermograms (B) and TGA curves (C) of poly(S-*r*-NB-AA) and poly(S-*net*-NB-AA) with increasing sulfur content. Full sulfur conversion was found up to 40 wt % of added sulfur in the cross-linking step, while the T_g decreased with increasing added amount of sulfur. $T_{5\%}$ also decreased with increasing sulfur content of poly(S-*net*-NB-AA). The inset shows the magnified area from 200 to 250 °C; dashed line: 95 wt %. D) T_g and $T_{5\%}$ plotted against determined sulfur content of poly(S-*net*-NB-AA). A linear correlation was found and approximated with a linear fit, indicating tunability of thermal properties of poly(S-*net*-NB-AA).

reaction of poly(S-*r*-NB-AA) with benzyl mercaptan can be found in the SI. Due to the dynamic nature of the S–S bond in polysulfides, a dynamic covalent polymerization approach was employed to create a cross-linked sulfur network with predictable sulfur content from poly(S-*r*-NB-AA) with a second inverse vulcanization step on the introduced allyl groups. Poly(S-*r*-NB-AA) were dry mixed with 20, 40, 60, 80, 100 wt % elemental sulfur, respectively and heated to 150 °C under stirring for 4 h (refer to Figure 5A). Weight percentages are given in relation to the total mass of poly(S-*r*-NB-AA). The resulting networked materials (poly(S-*net*-NB-AA)) were found to be hardly soluble in THF, dichloromethane, acetone, and ethanol regardless of the amount of added sulfur (refer to SI, Figure S37). The final sulfur contents of poly(S-*net*-NB-AA), after subsequent cross-linking with additional 20–100 wt % sulfur, were determined via elemental analysis and the results are summarized in Table 2. Full elemental composition (N, C, H, S) of poly(S-*r*-NB-AA) and poly(S-net-NB-AA) can be found in the Supporting Information (refer to Figure S38 and Table S3).

The consumption of elemental sulfur was evaluated using DSC, showing a complete conversion of sulfur for samples with 20 and 40 wt % added sulfur. Increasing the sulfur content in the feed further, resulted in residual crystalline sulfur in the material which extended from 60 to 100 wt % of added sulfur (refer to Figure 5B). The crystallinity of the materials was determined via DSC by calculating the melting enthalpy through integration of the sulfur melting peak. Comparison of the melting enthalpy of poly(S-*net*-NB-AA) with that of pure elemental sulfur allowed for an estimation of the crystallinity of the obtained materials (refer to SI, Table S4). The T_g of poly(S-*net*-NB-AA) decreased with increasing sulfur content, which can be explained by lengthening of polysulfide chains.[61] TGA of poly(S-*net*-NB-AA) with different sulfur contents showed the occurrence of one major decomposition step in the range of 200 to 500 °C, which can be attributed to the decomposition of polysulfur species (refer to Figure 5C). Notably, networked poly(S-*net*-NB-AA) did not fully decompose at temperatures up to 900 °C, showcasing enhanced thermal stability of the presented sulfur material. Interestingly, thermal properties of poly(S-*net*-NB-AA) were found to be directly related to the sulfur content of the material. Both T_g and thermal stability seemed to decrease linearly with increasing amount of sulfur found in poly(S-*net*-NB-AA) (refer to Figure 5D). This allows precise prediction and tunability of thermal material properties via efficient cross-linking of poly(S-*r*-NB-AA) with dynamic covalent polymerization utilizing elemental sulfur.

Table 2: Elemental analysis of poly(S-*r*-NB-AA) and poly(S-*net*-NB-AA) networked with additional sulfur. To 100 mg poly(S-*r*-NB-AA), the respective amounts of elemental sulfur were added, and the mixture was heated to 150 °C for 4 h.

Material	Added sulfur/ wt %	Polymer sulfur content/ wt %	Crystallinity /%
poly(S-*r*-NB-AA)	–	35 ± 3.1	–
poly(S-*net*-NB-AA)	20	47 ± 0.4	–
poly(S-*net*-NB-AA)	40	57 ± 1.4	–
poly(S-*net*-NB-AA)	60	67 ± 0.1	1.34
poly(S-*net*-NB-AA)	80	72 ± 2.0	4.29
poly(S-*net*-NB-AA)	100	76 ± 0.2	5.40

Conclusion

Inverse vulcanization of norbornenyl pentafluorophenyl ester (NB-PFPE) with elemental sulfur was reported. The resulting poly(S-*r*-NB-PFPE) was employed as a platform material for amidation, taking advantage of the active ester functionality derived from PFP esters. Amidation of poly(S-*r*-NB-PFPE) was conducted in solution under mild conditions with three different primary amines: First, α-amino-ω-methoxy poly(ethylene glycol) (Amino-mPEG), aminopropyl trimethoxy silane (APTMS), and allylamine (AA). Poly(S-*r*-NB-Amino-mPEG) formed spherical nanoscale particles, when exposed to aqueous media as confirmed by DLS and cryo-TEM measurements. Second, poly(S-*r*-NB-PFPE) was modified with APTMS, allowing exploitation of silane coupling chemistry. Surface coatings prepared by spin-coating of poly(S-*r*-NB-APTMS) on silicon wafers resulted in homogeneous, hydrophobic, and colored surfaces. Additionally, siloxane condensation of high sulfur-containing poly(S-*r*-NB-APTMS) allowed the preparation of spherical silica-sulfur particles as an efficient mercury adsorbent. For initial concentrations of 1–100 ppm Hg^{2+}, over 99 % of mercury could be removed from aqueous solutions by 100 mg silica-sulfur particles. Finally, synthesis of an unsaturated inverse vulcanized material was reported, available via amidation of poly(S-*r*-NB-PFPE) with AA. Glass transition temperature and thermal stability of poly(S-*r*-NB-AA) were precisely tuned by additional cross-linking in a subsequent inverse vulcanization step with elemental sulfur. The straightforward synthesis strategy presented in this work demonstrates the versatility of poly(S-*r*-NB-PFPE) as platform material toward a wide range of specialized applications, such as release systems, heavy metal remediation, antibacterial surfaces, lacquers, and high sulfur content materials with tunable thermal properties.

Supporting Information

The authors have cited additional references within the Supporting Information.[13,35,36,42,63]

Acknowledgements

The authors would like to thank Nicole Klaassen and Dr. Ute Schwotzer for conducting EA and CV-AAS measurements, respectively. Simon Barth and Angela Deutsch are acknowledged for surface area determination via BET measurements. The authors acknowledge funding from the Helmholtz Foundation program "Materials System Engineering" at the Karlsruhe Institute of Technology (KIT) as

well as the support via the Helmholtz Association. A.S. and F.H.S. are grateful for support from the DFG within the SFB 1278 "PolyTarget" (project number 316213987, project B04). The cryo-TEM/TEM facilities of the Jena Center for Soft Matter (JCSM) were established with a grant from the German Research Council (DFG) and the European Fonds for Regional Development (EFRE). Open Access funding enabled and organized by Projekt DEAL.

Conflict of Interest

The authors declare no conflict of interest.

Data Availability Statement

The raw data of the manuscript and the Supporting Information is publicly available in the RADAR4Chem Repository under the following DOI: 10.22000/PgmZKMHOGVgAvTnS.[62]

Keywords: Inverse vulcanization · Sulfur · Active ester · Mercury remediation · Post-polymerization modification

[1] T. Lee, P. T. Dirlam, J. T. Njardarson, R. S. Glass, J. Pyun, *J. Am. Chem. Soc.* **2022**, *144*, 5.
[2] M. J. King, W. G. Davenport, M. S. Moats, *Sulfuric acid manufacture. Analysis, control, and optimization*, Elsevier, Amsterdam **2013**.
[3] M. Akiba, *Prog. Polym. Sci.* **1997**, *22*, 475.
[4] P. Devendar, G.-F. Yang, *Top. Curr. Chem.* **2017**, *375*, 82.
[5] B. Zhang, H. Gao, P. Yan, S. Petcher, T. Hasell, *Mater. Chem. Front.* **2020**, *4*, 669.
[6] W. J. Chung, J. J. Griebel, E. T. Kim, H. Yoon, A. G. Simmonds, H. J. Ji, P. T. Dirlam, R. S. Glass, J. J. Wie, N. A. Nguyen, et al., *Nat. Chem.* **2013**, *5*, 518.
[7] J. J. Griebel, G. Li, R. S. Glass, K. Char, J. Pyun, *J. Polym. Sci. Part A* **2015**, *53*, 173.
[8] D. J. Parker, H. A. Jones, S. Petcher, L. Cervini, J. M. Griffin, R. Akhtar, T. Hasell, *J. Mater. Chem. A* **2017**, *5*, 11682.
[9] M. J. H. Worthington, R. L. Kucera, I. S. Albuquerque, C. T. Gibson, A. Sibley, A. D. Slattery, J. A. Campbell, S. F. K. Alboaiji, K. A. Muller, J. Young, et al., *Chemistry* **2017**, *23*, 16219.
[10] A. Hoefling, Y. J. Lee, P. Theato, *Macromol. Chem. Phys.* **2017**, *218*, 1600303.
[11] a) M. J. H. Worthington, M. Mann, I. Y. Muhti, A. D. Tikoalu, C. T. Gibson, Z. Jia, A. D. Miller, J. M. Chalker, *Phys. Chem. Chem. Phys.* **2022**, *24*, 12363; b) M. P. Crockett, A. M. Evans, M. J. H. Worthington, I. S. Albuquerque, A. D. Slattery, C. T. Gibson, J. A. Campbell, D. A. Lewis, G. J. L. Bernardes, J. M. Chalker, *Angew. Chem. Int. Ed.* **2016**, *55*, 1714.
[12] J. M. Scheiger, C. Direksilp, P. Falkenstein, A. Welle, M. Koenig, S. Heissler, J. Matysik, P. A. Levkin, P. Theato, *Angew. Chem. Int. Ed.* **2020**, *59*, 18639.
[13] A. P. Grimm, J. M. Scheiger, P. W. Roesky, P. Théato, *Polym. Chem.* **2022**.
[14] a) J. Molineux, T. Lee, K. J. Kim, K.-S. Kang, N. P. Lyons, A. Nishant, T. S. Kleine, S. W. Durfee, J. Pyun, R. A. Norwood, *Adv. Opt. Mater.* **2024**, *12*; b) T. S. Kleine, T. Lee, K. J. Carothers, M. O. Hamilton, L. E. Anderson, L. Ruiz Diaz, N. P. Lyons, K. R. Coasey, W. O. Parker, L. Borghi, et al., *Angew. Chem. Int. Ed.* **2019**, *58*, 17656; c) J. J. Griebel, S. Namnabat, E. T. Kim, R. Himmelhuber, D. H. Moronta, W. J. Chung, A. G. Simmonds, K.-J. Kim, J. van der Laan, N. A. Nguyen, et al., *Adv. Mater.* **2014**, *26*, 3014; d) J. M. Scheiger, P. Théato, in *Sulfur-containing polymers. From synthesis to functional materials* (Eds.: X.-H. Zhang, P. Théato), Wiley-VCH, Weinheim **2021**, pp. 305–338.
[15] S. J. Tonkin, N. Le Pham, J. R. Gascooke, M. R. Johnston, M. L. Coote, C. T. Gibson, J. M. Chalker, *Adv. Opt. Mater.* **2023**, *11*.
[16] a) Z. Deng, A. Hoefling, P. Théato, K. Lienkamp, *Macromol. Chem. Phys.* **2018**, *219*, 1700497; b) J. A. Smith, R. Mulhall, S. Goodman, G. Fleming, H. Allison, R. Raval, T. Hasell, *ACS Omega* **2020**, *5*, 5229.
[17] V. S. Wadi, K. K. Jena, S. Z. Khawaja, V. M. Ranagraj, S. M. Alhassan, *RSC Adv.* **2019**, *9*, 4397.
[18] J. Bao, K.-S. Kang, J. Molineux, D. J. Bischoff, M. E. Mackay, J. Pyun, J. T. Njardarson, *Angew. Chem. Int. Ed.* **2024**, *63*, e202315963.
[19] a) M. Mann, J. E. Kruger, F. Andari, J. McErlean, J. R. Gascooke, J. A. Smith, M. J. H. Worthington, C. C. C. McKinley, J. A. Campbell, D. A. Lewis, et al., *Org. Biomol. Chem.* **2019**, *17*, 1929; b) A. S. M. Ghumman, R. Shamsuddin, R. Sabir, A. Waheed, A. Sami, H. Almohamadi, *RSC Adv.* **2023**, *13*, 7867.
[20] a) Y. Xin, H. Peng, J. Xu, J. Zhang, *Adv. Funct. Mater.* **2019**, *29*, 1808989; b) S. J. Tonkin, C. T. Gibson, J. A. Campbell, D. A. Lewis, A. Karton, T. Hasell, J. M. Chalker, *Chem. Sci.* **2020**, *11*, 5537; c) N. A. Lundquist, A. D. Tikoalu, M. J. H. Worthington, R. Shapter, S. J. Tonkin, F. Stojcevski, M. Mann, C. T. Gibson, J. R. Gascooke, A. Karton, et al., *Chemistry* **2020**, *26*, 10035.
[21] a) P. T. Dirlam, A. G. Simmonds, T. S. Kleine, N. A. Nguyen, L. E. Anderson, A. O. Klever, A. Florian, P. J. Costanzo, P. Theato, M. E. Mackay, et al., *RSC Adv.* **2015**, *5*, 24718; b) A. Hoefling, D. T. Nguyen, Y. J. Lee, S.-W. Song, P. Theato, *Mater. Chem. Front.* **2017**, *1*, 1818; c) H. Wang, B. Zhang, R. Dop, P. Yan, A. R. Neale, L. J. Hardwick, T. Hasell, *J. Power Sources* **2022**, *545*, 231921; d) T. Zhang, F. Hu, W. Shao, S. Liu, H. Peng, Z. Song, C. Song, N. Li, X. Jian, *ACS Nano* **2021**, *15*, 15027.
[22] D. H. Kim, W. Jang, K. Choi, J. S. Choi, J. Pyun, J. Lim, K. Char, S. G. Im, *Sci. Adv.* **2020**, *6*, eabb5320.
[23] X. Wu, J. A. Smith, S. Petcher, B. Zhang, D. J. Parker, J. M. Griffin, T. Hasell, *Nat. Commun.* **2019**, *10*, 647.
[24] J. Jia, J. Liu, Z.-Q. Wang, T. Liu, P. Yan, X.-Q. Gong, C. Zhao, L. Chen, C. Miao, W. Zhao, et al., *Nat. Chem.* **2022**.
[25] K.-S. Kang, C. Olikagu, T. Lee, J. Bao, J. Molineux, L. N. Holmen, K. P. Martin, K.-J. Kim, K. H. Kim, J. Bang, et al., *J. Am. Chem. Soc.* **2022**.
[26] J. M. M. Pople, T. P. Nicholls, N. Le Pham, W. M. Bloch, L. S. Lisboa, M. V. Perkins, C. T. Gibson, M. L. Coote, Z. Jia, J. M. Chalker, *J. Am. Chem. Soc.* **2023**.
[27] Y. Zhang, K. M. Konopka, R. S. Glass, K. Char, J. Pyun, *Polym. Chem.* **2017**, *8*, 5167.
[28] K.-S. Kang, A. Phan, C. Olikagu, T. Lee, D. A. Loy, M. Kwon, H. Paik, S. J. Hong, J. Bang, W. O. Parker, et al., *Angew. Chem. Int. Ed.* **2021**, *60*, 22900.
[29] I. Gomez, A. F. de Anastro, O. Leonet, J. A. Blazquez, H.-J. Grande, J. Pyun, D. Mecerreyes, *Macromol. Rapid Commun.* **2018**, *39*, e1800529.
[30] C. P. Ambulo, K. J. Carothers, A. Hollis, H. N. Limberg, L. Sun, C. J. Thrasher, M. E. McConney, N. P. Godman, *Macromol. Rapid Commun.* **2023**, e2200798.
[31] N. Q. Tufts, N. C. Chiu, E. N. Musa, T. C. Gallagher, D. B. Fast, K. C. Stylianou, *Chemistry* **2023**, e202203177.

[32] J. M. Scheiger, M. Hoffmann, P. Falkenstein, Z. Wang, M. Rutschmann, V. W. Scheiger, A. Grimm, K. Urbschat, T. Sengpiel, J. Matysik, et al., *Angew. Chem.* **2022**.
[33] D. Wang, Z. Tang, R. Huang, H. Li, C. Zhang, B. Guo, *Macromolecules* **2022**.
[34] P. Theato, *J. Polym. Sci. Part A* **2008**, *46*, 6677.
[35] K. Zhang, M. A. Lackey, Y. Wu, G. N. Tew, *J. Am. Chem. Soc.* **2011**, *133*, 6906.
[36] M. Rémy, I. Nierengarten, B. Park, M. Holler, U. Hahn, J.-F. Nierengarten, *Chemistry* **2021**, *27*, 8492.
[37] S. H. Je, H. J. Kim, J. Kim, J. W. Choi, A. Coskun, *Adv. Funct. Mater.* **2017**, *27*, 1703947.
[38] T. Baran, A. Duda, S. Penczek, *J. Polym. Sci. Polym. Chem. Ed.* **1984**, *22*, 1085.
[39] M. Eberhardt, R. Mruk, R. Zentel, P. Théato, *Eur. Polym. J.* **2005**, *41*, 1569.
[40] a) Y. Zhang, N. G. Pavlopoulos, T. S. Kleine, M. Karayilan, R. S. Glass, K. Char, J. Pyun, *J. Polym. Sci. Part A* **2019**, *57*, 7; b) L. J. Dodd, W. Sandy, R. Dop, B. Zhang, A. Lunt, D. R. Neill, T. Hasell, *Polym. Chem.* **2023**.
[41] a) J. A. Smith, X. Wu, N. G. Berry, T. Hasell, *J. Polym. Sci. Part A* **2018**, *56*, 1777; b) L. J. Dodd, Ö. Omar, X. Wu, T. Hasell, *ACS Catal.* **2021**, *11*, 4441.
[42] Y. A. Wickramasingha, F. Stojcevski, D. J. Eyckens, D. J. Hayne, J. M. Chalker, L. C. Henderson, *Macromol. Mater. Eng.* **2024**, *309*.
[43] P. Yan, H. Wang, L. J. Dodd, T. Hasell, *Commun. Mater.* **2023**, *4*.
[44] Y. Zhang, R. S. Glass, K. Char, J. Pyun, *Polym. Chem.* **2019**, *10*, 4078.
[45] J. M. Dust, Z. H. Fang, J. M. Harris, *Macromolecules* **1990**, *23*, 3742.
[46] M. Rozenberg, A. Loewenschuss, Y. Marcus, *Spectrochim. Acta Part A* **1998**, *54*, 1819.
[47] X. Y. D. Soo, Z. M. Png, X. Wang, M. H. Chua, P. J. Ong, S. Wang, Z. Li, D. Chi, J. Xu, X. J. Loh, et al., *ACS Appl. Polym. Mater.* **2022**, *4*, 2747.
[48] D. Craig, J. M. Newton, *Int. J. Pharm.* **1991**, *74*, 33.
[49] G. W. Ehrenstein, G. Riedel, P. Trawiel, *Praxis der thermischen Analyse von Kunststoffen*, Hanser, München **2003**.
[50] H. Shin, J. Kim, D. Kim, V. H. Nguyen, S. Lee, S. Han, J. Lim, K. Char, *J. Mater. Chem. A* **2018**, *6*, 23542.
[51] M. Brehm, J. M. Scheiger, A. Welle, P. A. Levkin, *Adv. Mater. Interfaces* **2020**, *7*.
[52] C. Xia, Y. Peng, Y. Yi, H. Deng, Y. Zhu, G. Hu, *J. Magn. Magn. Mater.* **2019**, *474*, 424.
[53] Y. Bai, Q. Dong, Y. Shao, Y. Deng, Q. Wang, L. Shen, D. Wang, W. Wei, J. Huang, *Nat. Commun.* **2016**, *7*, 12806.
[54] Z. Sasan Narkesabad, R. Rafiee, E. Jalilnejad, *Sci. Rep.* **2023**, *13*, 3670.
[55] F. Yan, J. Jiang, X. Chen, S. Tian, K. Li, *Ind. Eng. Chem. Res.* **2014**, *53*, 11884.
[56] J. M. Chalker, M. Mann, M. J. H. Worthington, L. J. Esdaile, *Org. Mater.* **2021**, *03*, 362.
[57] S. M. Mobin, V. Mishra, D. K. Rai, K. Dota, A. K. Dharmadhikari, J. A. Dharmadhikari, D. Mathur, P. Mathur, *Dalton Trans.* **2015**, *44*, 1933.
[58] M. K. Denk, *Eur. J. Inorg. Chem.* **2009**, *2009*, 1358.
[59] E. Reinhard, E. A. Khan, A. Oguz Akyuz, G. Johnson, *Color Imaging*, A. K. Peters, CRC Press **2008**.
[60] N. K. Singha, M. I. Gibson, B. P. Koiry, M. Danial, H.-A. Klok, *Biomacromolecules* **2011**, *12*, 2908.
[61] J. J. Dale, S. Petcher, T. Hasell, *ACS Appl. Polym. Mater.* **2022**.
[62] A. Grimm, *Inverse Vulcanization of Activated Norbornenyl Esters - A Versatile Platform for Functional Sulfur Polymers*, Théato, Patrick **2024**.
[63] a) L. K. Kostanski, D. M. Keller, A. E. Hamielec, *J. Biochem. Biophys. Methods* **2004**, *58*, 159; b) P. A. Woodfield, Y. Zhu, Y. Pei, P. J. Roth, *Macromolecules* **2014**, *47*, 750; c) N. Han, W. Cho, J. H. Hwang, S. Won, D.-G. Kim, J. J. Wie, *Polym. Chem.* **2023**; d) M. W. Thielke, L. A. Bultema, D. D. Brauer, B. Richter, M. Fischer, P. Theato, *Polymer* **2016**, *8*; e) C. Copeland, R. J. Conway, J. J. Patroni, R. V. Stick, *Aust. J. Chem.* **1981**, *34*, 555.

Manuscript received: June 11, 2024
Accepted manuscript online: June 19, 2024
Version of record online: August 2, 2024